Study of organic aerosol of phytogenic origin with fluorescent lidar

A.I. Grishin,[1] G.M. Krekov,[1] M.M. Krekova,[1] G.G. Matvienko,[1] A.Ya. Sukhanov,[1] V.I. Timofeev,[2] N.L. Fateyeva,[1] and A.A. Lisenko[1]

[1]*Institute of Atmospheric Optics, Siberian Branch of the Russian Academy of Sciences, Tomsk*
[2]*Lomonosov Moscow State University, Moscow*

Received January 16, 2007

The paper discusses the results of complex studies, dealing with use of the phenomenon of laser-induced fluorescence (LIF) for remote monitoring of the state of vegetation cover. We outline the specific features of functional scheme of new-generation fluorescent lidar, enabling measurement of practically continuous LIF spectra from distance of a few tens of meters. We demonstrate the potentialities of lidar both for analysis of traditional spectra of chlorophyll *a* in wood plants and for identification of bioaerosols, being products of the secondary metabolism of plants. The experimental measurements are supported by theoretical-numerical analysis of applicability limits of the developed methods of identification under conditions of the real turbid atmosphere.

Introduction

Laser-induced fluorescence (LIF), as an optical phenomenon, provides a basis for creation of efficient means of remote detection and identification of a wide range of molecular compounds including environmentally hazardous ones.[1] It should be noted that in analytical photochemistry and photobiology the methods of *in situ* fluorescent spectroscopy have been successfully used for already long time. Detailed list of these results (over 500 items) is overviewed in Ref. 2.

First successful experiments in remote lidar sensing on the basis of broadband LIF were performed in the works on the control of chlorophyll and phytoplankton content in near-surface layer of the ocean.[3–5] Attempts to use fluorescent methods for diagnostics of biogenic aerosol in the troposphere failed at the first stages.[6] However, introduction of new-generation femtosecond laser sources[7,8] and new instruments of LIF stimulation[9,10] into practice of remote sensing has opened new possibilities of fluorescent lidars in the atmospheric optics studies.[11]

Most fruitful field of fluorescent lidar (FLIDAR) applications is still the monitoring of vegetation cover of planet, including wide range of active fluorophores, responding to metabolic processes.[12,13] In recent years, a very urgent problem has been the issue of implementation of efficient remote methods of detection and identification of biologic aerosols hazardous for human health (spores, bacteria, viruses, etc.).

As laboratory *in situ* measurements show,[14,15] LIF offers the highest sensitivity compared with other methods. The lidar measurements under real atmospheric conditions are yet restricted to very short paths.[16,17] These restrictions are associated not only with small spectral intensity of LIF, but also with difficulties of correct interpretation of obtained LIF spectra. The point is that the LIF spectra of the class of proteins and even living microorganisms frequently have identical qualitative character. The spectra in the dense near-ground atmosphere are very broad and have no characteristic features. Moreover, on the long atmospheric paths such as in helicopter sensing scheme,[18] the LIF spectra have a tendency of distortion and smoothing due to interference and multiple scattering in surrounding natural aerosol. Technically, these difficulties are overcome by use of "*pump-and-probe*" method,[10,11] multispectral fluorescence,[19] multi-photon LIF,[20] effect of saturation of fluorescence,[21] and high-frequency LIF amplitude modulation.[22]

From methodical viewpoint, good promises are associated with use of the algorithms of artificial neural networks.[23,24]

However, as noted by Dolenko et al.,[23] the accuracy of classification and recognition of the sought images (fluorophores) depends significantly on the accuracy of the processed information. In this regard, below we tried to quantitatively estimate the limits of possible transformation of typified spectra of the broadband LIF under conditions of the real atmospheric sensing paths. The experimental measurements are made on the basis of modified fluorescent lidar. The quantitative estimates are obtained using new algorithms of solution of nonstationary equation of transfer of broadband LIF radiation by the Monte Carlo method.

1. Modification of fluorescent lidar

As noted above, among the spectroscopic effects attractive from viewpoint of monitoring of physiological functions of the plants and usable for implementation

0235-6880/07/04 294-09 $02.00

in lidar systems, we should highlight the methods of analysis of fluorescence of plant tissues. In particular, the fluorescence of chlorophyll is widely used for analysis of photosynthetic system of plants. The photosynthetic function of the leaf and its pigment system are characterized by high variability degree. These variations are associated with regularities of ontogenesis of the leaf and wood organism and with influence of extremal environmental factors, substantially altering the magnitude and rhythm of growth processes, intensity of photosynthesis, and characteristics of pigment system.

The plant pigment system and, in particular, the chlorophyll content, besides being the criterion of plant assessment, simultaneously indirectly characterizes the state of environment. This indicates that the use of this characteristic as a marker parameter is promising. Modern methods of the biochemical determination of the quantitative chlorophyll content are quite laborious and time consuming. In addition, during determination of chlorophyll content in different dissolutions, there takes place the breakup of the native structure of leaf pigment system, creating difficulties in interpretation of the obtained results. Recently, of concern has been the problem of quantitative remote control of content and dynamics of variations of the secondary metabolites within the vegetation cover, which reflect the conditions of plant development. All this indicates that new methods should be invoked in the context of fast monitoring of the state and organization of plant pigment system.

First remote measurements of laser-induced fluorescence of chlorophyll of wood plants were performed by ourselves with use of lidar, recording LIF signals at fixed wavelengths 532, 685, and 740 nm.[16,26] The latter two wavelengths are associated with fluorescence of chlorophyll of *a* and *b* types respectively.

This prototype of fluorescent lidar[16,26] operated as follows. The pulse of radiation at wavelength 532 nm (the second harmonic for yttrium aluminum garnet) is directed to the sensed volume. Under influence of the incident light in Stokes region of the spectrum, spontaneous fluorescence of an element of vegetation cover or aerosol of phytogenic origin is excited. Part of the radiation is intercepted with use of receiving telescope and is directed via fiber to the input of spectrophotometer, assembled according to the autocollimation scheme. As a result, we obtained quite abundant data on dynamics of the behavior of fluorescent characteristics for typical representatives of the wood plants of Siberian region: cedar, pine, and birch. The samples were placed at distance 70 m from the laser radar and exposed to illumination on average twice weekly during dark part of the day. We observed the variations of fluorescent characteristics of chlorophyll from time of cutting the samples to the stage corresponding to complete fading of the plants. A total of 35 measurement cycles were performed, and the samples were changed 6 times for period from April 20 to September 23, 1999.

To obtain larger information and, primarily, to increase the spectral capabilities of lidar, we tried to perform its cardinal modification.[36] Below we will address most notable points of this modification.

In *initial* lidar version, the receiving-transmitting part was assembled according to biaxial scheme, based on the glass optics. Mainly, this was because we used as the source of radiation the first and second harmonics of laser based on yttrium aluminum garnet (YAG) with the corresponding wavelengths 1064 and 532 nm, while the luminescence spectrum was measured in the region 670–850 nm.

Specifications of the initial lidar version

Energy of laser pulse (first harmonic), mJ	10–20
Wavelength of radiation, nm	1064, 532
Duration of radiation pulses, ns	10–15
Divergence of radiation beam, mrad	6
Diameter of receiving telescopes, cm	15
Field of view angle, mrad	9
ADC digit capacity, bit	8
Discretization frequency, MHz	20

A modified version of the fluorescent lidar is based on the mirror optics and assembled according to the coaxial scheme. Glass optics was changed to the mirror one due to widening the spectral range of both laser radiation and fluorescent signal from visible to ultraviolet range (the reasons are explained below). The use of coaxial scheme instead of biaxial one partially resolves difficulties associated with determination of the lidar form-factor. To widen the functional range of the lidar operation, ultraviolet channels of excitation, 266 and 355 nm, have been realized, allowing a considerably increase of the range of the studied fluorophores. The spectral sweep unit of the received LIF signal is activated. The functional scheme of the modified fluorescent lidar is presented in Fig. 1.

The transmitting part consists of the laser emitter, collimator expanding the laser beam, and plane mirrors ensuring coaxiality in adjustment of optical axes of the transmitter and the receiver. The receiving part is presented by the Cassegrain telescope, formed by a parabolic mirror and a counter-reflecting mirror.

The whole receiving-transmitting unit is placed on rotating mechanical column, representing the main element of the guidance system (GS). By controlling the rotation of column and scan in elevation angle of receiver-transmitter, the pointing in a given direction or observations in a chosen region of three-dimensional space is conducted. In addition, during measurement GS maintains the axis of directional pattern of the receiving-transmitting channel at a given point of the space with the required accuracy.

The laser source radiation is directed through the collimator and plane mirrors to the object under study. Radiation from the object is received by telescope and, via fiber, is transferred to the spectral selector, formed by the own collimator and diffraction grating.

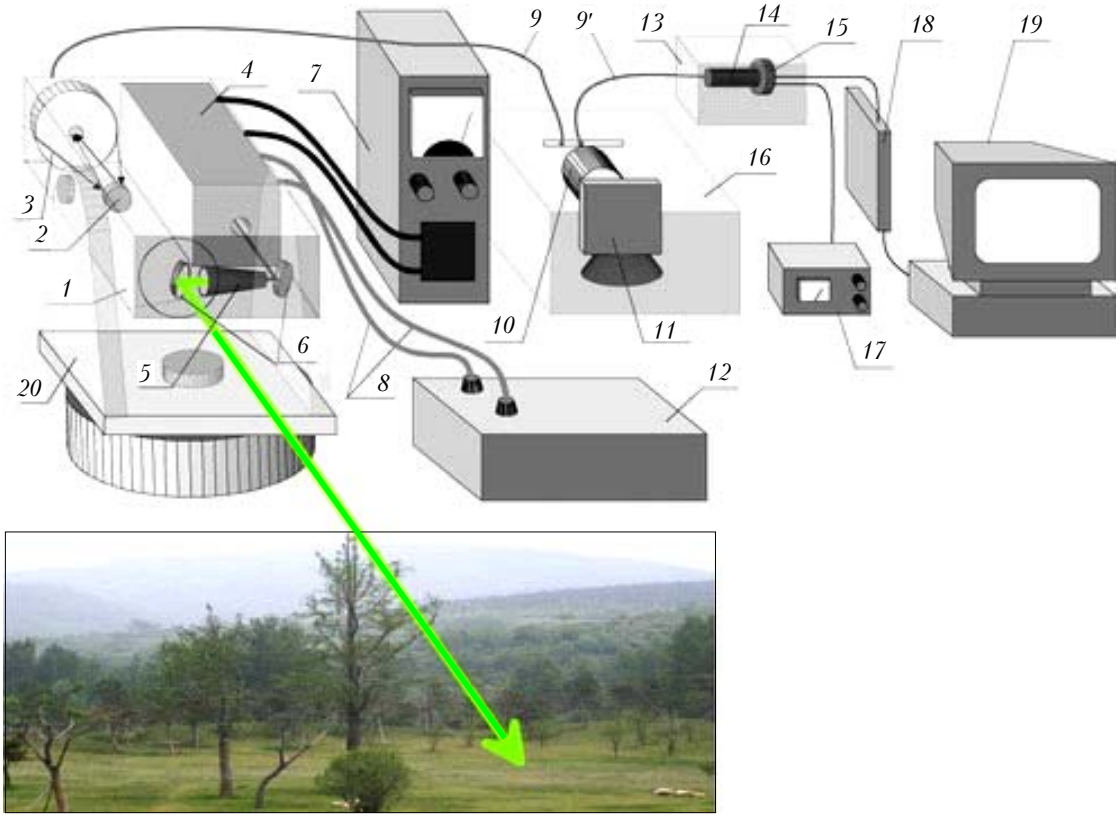

Fig. 1. Functional scheme of modified fluorescent lidar: *1* is receiver-transmitter; *2* is counter-reflector of receiving telescope; *3* is parabolic mirror; *4* is laser emitter; *5* is collimator; *6* is plane mirror; *7* is power supply of laser; *8* is hoses of laser cooling; *9*, *9′* are fibers; *10* is objective of the polychromator; *11* is diffraction grating; *12* is cooling unit; *13* is photodetector unit; *14* is PMT; *15* is bleeder; *16* is polychromator; *17* is power supply of PMT; *18* is ADC; *19* is computer; *20* is rotating column.

Radiation, decomposed to wavelengths, is directed via fibers to photodetector unit composed of a number of PMTs. The electric signals, produced by PMT, are converted in the analog-to-digital converter and go to computer for final processing.

Noteworthy, when a chamber on the basis of a charge-coupled device (CCD) array is used, its connection to the output of the polychromator is direct, i.e., free of additional fibers.

Specifications of the modified lidar

Energy of laser pulse (first harmonic), mJ	10–20
Wavelength of radiation, nm	1064, 532, 355, 266
Duration of radiation pulses, ns	5–15
Divergence of radiation beam, mrad	1
Diameter of receiving telescope, cm	20
Relative orifice	1–5
Field of view angle, mrad	2
ADC digit capacity, bit	16
Discretization frequency, MHz	100

2. Biophysical aspects of laser-induced fluorescence

When designing and improving the fluorescent lidar, we pursued the possibility of simultaneous measurement of optical characteristics of vegetation, its secondary metabolites, and, at the final stage, bioaerosols. In this case, the wavelength of radiation turns to be the most important parameter of the laser radar.

When plants are exposed to UV or visible laser radiation, the fluorescence of green leafs is caused by luminescing substances of plant cells, main of which are chlorophylls, phycobilines, alkaloids, and flavonoids. A typical spectrum of green leaf fluorescence[27] in the case of its excitation by a 355 nm laser is shown in Fig. 2.

The spectral intensity of LIF emission from cells in the blue–green region is determined by different groups of luminescing substances. These substances include caratinoids and tryptophan-containing albumens, fluorescing in the region 420–460 nm, and oxidized flavoproteins and coenzymes (400–500 nm), as well as the products of lipid peroxidizing (lipofuscin) 500–630 nm. From record of the fluorescent spectrum we see that it also has a characteristic maxima at 685 and 740 nm. It is well known that the 685 nm band belongs to pigment-albuminous compounds of phytosystem II (PS II) of photosynthesizing system (PSS) of plant, and that the band in the region 740 nm is more complex and characterizes the work of PS I. Note that, due to absorption of light, PS I causes oxidizing of electron

carriers and recombination of nicotinamide-adenine dinucleotide phosphate (NADP), while FS II, due to absorption of light, ensures water decomposition with release of oxygen and recombination of electron carriers. The luminescence of photosynthesizing organisms is emitted by chlorophyll, the main pigment of PSS, responsible for the above-mentioned bands of 685 and 740 nm.

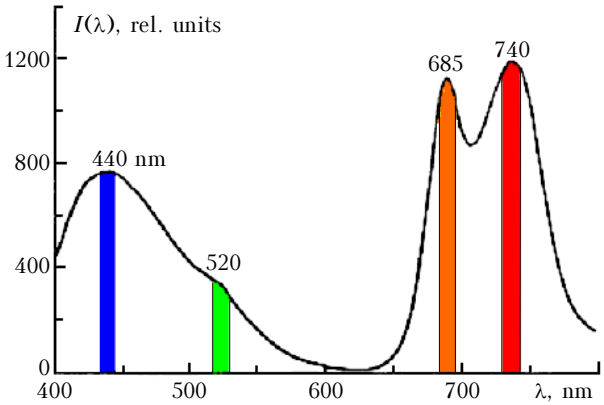

Fig. 2. Typical fluorescence spectrum of a green leaf.

From the aforesaid it is clear that an excitation wavelength a little shorter than 670 nm is sufficient for observation of chlorophyll luminescence. At the same time, it is obvious that, to induce the luminescence spectra of albumens, radiation with wavelength no longer than 300 nm is required. It is well known, for instance, that most of the secondary metabolites effectively absorb in UV spectral range, and fluoresce in the near-UV and visible regions of the spectrum.

Thus, the optimal wavelength of laser source of fluorescent phytolidar must be in the range 260–270 nm. This requirement is ideally met by fourth harmonic of yttrium aluminum garnet laser at 266 nm. Therefore, in the modified version of the lidar, a provision was made for possibility of conversion of the main wavelength of YAG laser to both the second, third, and fourth harmonics. The latter was achieved by mounting an additional nonlinear element, based on BBO crystal, in the laser channel. Coefficient of conversion of the main harmonic to the fourth one is 10%.

3. Results of experimental measurements

In anthropogenic pollution of soils, a primary characteristic, even at small pollutant concentrations, is a change of fluorescent signal from tree crown. As was noted earlier,[28] deciduous plants have the highest sensitivity.

Figure 3*a* presents the results of measurements of fluorescent signal from birch leafs at λ = 685 and 740 nm.

Already the next day following the pollution of soil cover around birch root, the fluorescence signal, induced by laser radiation of 532 nm, increases by more than a factor of two for 685 and by almost 50% for λ = 740 nm. The period of plant adaptation to external effect lasts for 7–8 days, and then the level of fluorescence signals returns to initial values for both wavelengths. When the fourth harmonic of the YAG laser is used as a wavelength of excitation, aerosol of the phytogenic origin, having in its basis the products of the secondary metabolism, fluoresces more actively. The studied object was chosen to be the region over a separate tree (birch) at a distance of 70 m, and the height of the sensed region was 1 m higher than the tree crown. The intensity of release of the secondary metabolites positively correlates with degree of soil toxic pollution. However, the timescales of LIF growth, as a response to the toxic impact, are larger and equal to 5–7 days. At the same time, the

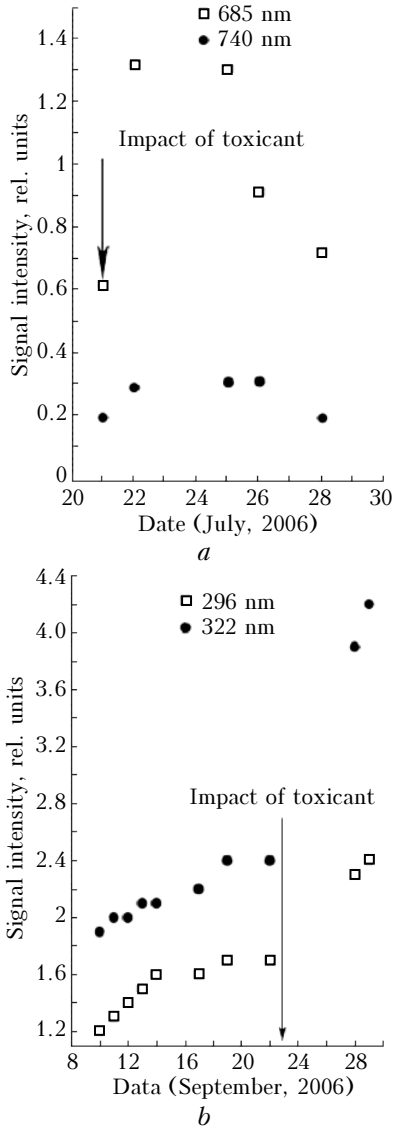

Fig. 3. Variation of fluorescence signal: from birch crown during anthropogenic pollution of soil by easily hydrolyzed nitrogen (*a*); and from aerosol component over birch during anthropogenic pollution of soils by derivatives of benzene (*b*).

LIF intensity increases less than for vegetation cover (in particular, at λ = 322 nm). This increase was 60%; while at λ = 296 nm, it was only 40% (Fig. 3*b*).

Thus, at anthropogenic pollution of soils, as the primary characteristic of the change of fluorescent component of signal from plant crown can be considered, followed by appearance of the secondary metabolites and, as a consequence, an increase of fluorescence signal from aerosol component in vicinity of the plant, further followed by a change of the structure of deciduous or coniferous cover. As a consequence, the return changes. The times of appearance of these features depend on concentrations of the polluting substance and the period between one and three days for fluorescence of the crown and between five and seven days for aerosol components. As was noted earlier,[28] the change of the reflection coefficient is observed only for strong damages and can be recorded no sooner than 5 days after appearance of polluting substance in the soil.

Using λ = 266 nm as an exciting radiation, we for the first time performed a series of measurements of entire fluorescence spectrum of the secondary metabolites in the range 270–335 nm for different plant physiological states. The measurements were performed every day starting from September 17, 2006, at nighttime, and their results are presented in Fig. 4. In order to create stress conditions, on September 23 we pour a large amount of toxicant on the ground below the tree. Until September 28, the mean level of fluorescence signal did not exceed the noise level characteristic for the period September 17–23. However, on September 28 and 29 the signal abruptly increased, especially in the spectral region 325 nm.

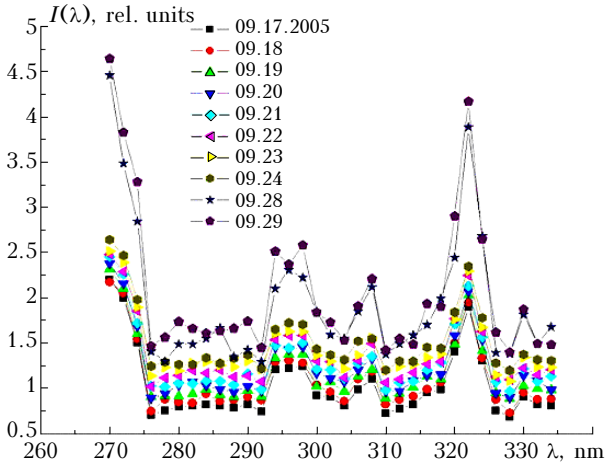

Fig. 4. A series of continuous spectra of fluorescence signal from the region above the birch, obtained in period September 17–29, 2005.

The qualitative analysis of the obtained family of the fluorescence spectra gave grounds to believe that the rapid increase of the LIF signals in the region 325 nm is associated with the increase of the concentration of 1H-Indole, one of the secondary metabolites typical in such cases, due to response of the birch to the stress effect. Then, for quantitative identification of LIF spectra, we used the results of the theory of the method of artificial neuron networks (ANN).

4. Identification of LIF spectra

In recent years, the method of artificial neural networks (ANN) was proved to be one of the most efficient tools of image recognition.[23, 29] Possibilities of the ANN method in solving one class of atmospheric optics problems were demonstrated in Refs. 30 and 31.

The neural networks represent a set of interrelated elements of neurons, each responding to the input impact with a certain output signal. Mathematically, a formal neuron can be described as follows:

$$y = \phi\left(\sum_{i=1}^{N} w_i x_i + w_0\right), \qquad (1)$$

where y is the output signal of neuron; ϕ is the activation function of neuron; w are the weighting coefficients; N is the number of inputs; x are the inputs; and w_0 is the threshold coefficient.

The intensity spectrum values serve as the inputs of this neuron network. The network has one output, which shows the possibility of recognition; this output may take a real value from 0 to 1. The spectrum is assumed to be recognized if the value is larger than 0.7 and not recognized otherwise. For training of the network, an algorithm of backward error propagation with a cross-check on a test sample is applied.[32]

Separate results of identification are shown in Fig. 5.

Maximum of LIF spectral curves in the region 325 nm, obtained on September 28 and 29, are confidently identified as a manifestation of indol (see a reference laboratory spectrum in Fig. 5). The other curves did not pass the identification test. This may be due either to low level of concentration of bioaerosols or to a marked level of atmospheric noise. This problem will be again addressed in section 5.

Note that the training sample was created by deviating the parameters (halfwidth, amplitude, and center) of Gauss function from the initial spectrum by a certain small amount in percent of initial values ($A_1 = 0.1 \cdot 10^{-2}$, $h_1 = 0.1 \cdot 10^{-3}$, $\sigma_1 = 0.2 \cdot 10^{-4}$; $A_2 = 0.2 \cdot 10^{-2}$, $h_2 = 0.2 \cdot 10^{-3}$, $\sigma_2 = 0.01 \cdot 10^{-2}$). It was assumed that in the case of identification, the network must output 0.95:

$$f(x) = A_1 \exp\left(-\frac{(x-h_1)^2}{2\sigma_1^2}\right) + A_2 \exp\left(-\frac{(x-h_2)^2}{2\sigma_2^2}\right), \qquad (2)$$

where A_1 and A_2 are the amplitudes of Gauss functions representing the spectrum; σ_1 and σ_2 are the halfwidths; and h_1 and h_2 are the centers.

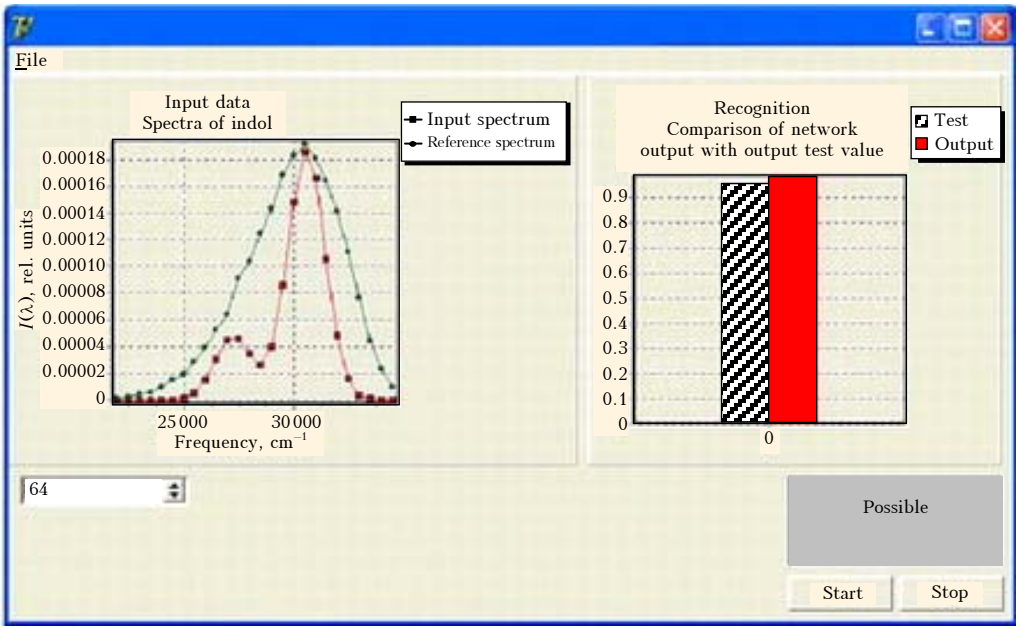

Fig. 5. Interface of identification of experimental spectrum, obtained on September 29, 2005 (see Fig. 4) by the ANN method.

5. Statistical modeling of laser-induced fluorescence of organic aerosol

The process of distribution of a short lidar signal at wavelengths of excitation of laser-induced fluorescence will be described following Ref. 25, by nonstationary radiative transfer equation (RTE) in 3D-space:

$$c^{-1}\frac{\partial I(\mathbf{r},\Omega,t)}{\partial t}+\Omega\nabla I(\mathbf{r},\Omega,t)=-\sigma(\mathbf{r},\lambda)I(\mathbf{r},\Omega,t)+$$

$$+\frac{1}{4\pi}\int_{4\pi}G_{\mathrm{M}}(\mathbf{r},\Omega',\Omega)I(\mathbf{r},\Omega',t)\,\mathrm{d}\Omega'+\Phi_0(\mathbf{r},t), \qquad (3)$$

where $I(\mathbf{r},\Omega,t)$ is the intensity of radiation at wavelength λ at point $\mathbf{r}(x,y,z)$ in direction Ω; $G_{\mathrm{M}}(\mathbf{r},\Omega',\Omega)$ is the volume coefficient of the directional elastic scattering; $\sigma(\lambda)$ is the total extinction coefficient at the wavelength λ, i.e.,

$$\sigma(\lambda)=\alpha(\lambda)+\sigma_{\mathrm{S}}(\lambda),$$

where $\alpha(\lambda)=\alpha_{\mathrm{M}}(\lambda)+\alpha_{\mathrm{F}}(\lambda)$, α_{M} is the coefficient of absorption by particles of the medium due to thermal dissipation; $\alpha_{\mathrm{F}}(\lambda)$ is the absorption by fluorophores; $\sigma_{\mathrm{S}}(\lambda)=\sigma_{\mathrm{M}}(\lambda)+\sigma_{\mathrm{R}}(\lambda)$; $\sigma_{\mathrm{M}}(\lambda)$ and $\sigma_{\mathrm{R}}(\lambda)$ are the coefficients of elastic and inelastic (Raman) scattering.

External source $\Phi_0(\mathbf{r},t)$ excites fluorophores with absorption coefficient $\alpha_{\mathrm{F}}(\lambda)$ at the wavelength of laser radiation.

The spectral intensity I_{F} of the subsequent emission of the fluorescent light at $\lambda'\in\Lambda$ (Λ is the spectral region of emission) will satisfy the equation

$$c^{-1}\frac{\partial I_{\mathrm{F}}(\mathbf{r},\Omega,\tau,\lambda')}{\partial\tau}+\Omega\nabla I_{\mathrm{F}}(\mathbf{r},\Omega,\tau,\lambda')=$$

$$=-[\sigma_{\mathrm{M}}(\mathbf{r},\lambda')+\alpha(\mathbf{r},\lambda)]I(\mathbf{r},\Omega,t)+$$

$$+\frac{1}{4\pi}\int_{4\pi}G_{\mathrm{M}}(\mathbf{r},\Omega',\Omega)I(\mathbf{r},\Omega',t)\,\mathrm{d}\Omega'+\Phi_{L_0}(\mathbf{r},\tau,\lambda,\lambda'), \qquad (4)$$

where

$$\Phi_{L_0}(\mathbf{r},\tau,\lambda,\lambda')=\frac{1}{4\pi}\eta(\lambda')\alpha_{\mathrm{F}}(\lambda)q(\tau)\int_{4\pi}I(\mathbf{r},\Omega,\tau,\lambda)\,\mathrm{d}\Omega$$

is the function of the internal LIF sources, distributed over the medium volume. Obviously,[25] it will depend on the intensity of the exciting radiation, quantum efficiency (quantum yield) of fluorescence $\eta(\lambda')$, and decay time $q(\tau)$.

As a result of solving the system of equations (3) and (4) by the Monte Carlo method,[25] we obtain an estimate of backscattered intensity of the fluorescent lidar in the neighborhood of the given detector.

As illustrative examples, we considered two model problems. The first problem is concerned with the estimate of the transformation of the LIF spectrum of chlorophyll *a*, induced by the second harmonic of YAG laser radiation on cedar samplings, growing under different development conditions. The second task was to estimate possible distortions of the fluorescence spectrum of indol due to complex atmospheric-optical conditions on a long sensing path.

The numerical solution of the system (3) and (4) provides a pattern of the spatiotemporal and spectral LIF distribution in the region of a given detector. Parameters of the detector and other boundary conditions, determining the region of the estimate of the sought functionals, correspond to the real construction of the above-mentioned fluorescent lidar, operating in the Laboratory of Lidar Methods, Institute of Atmospheric Optics SB RAS, with exception that the estimates are complimented with results for wide-angle reception.

All estimates are constructed in relative units, giving grounds to believe that the data for singly scattered signal exactly correspond to the lidar signal, described by the laser location equation. Actually existing multiple scattering distorts the signal, leading to biased estimate of the concentration of the sought fluorophore or even to its misidentification. As was noted earlier,[31] the integral quantum efficiency $\eta(\lambda')$ was taken to be constant at the level 0.03 because of the absence of refined data. Average quenching time was assumed to be in the range 5.0–10.0 ns, which for the coarse time grid of the signal resolution has no marked effect.

Figure 6*a* presents estimates of the spatially resolved spectra of LIF of chlorophyll *a* from the boundary layer of the homogeneous coniferous forest as functions of the penetration depth of the radar signal.

We took as the initial LIF signal, free of the multiple scattering, the experimental LIF spectrum, recorded from the edge of the forest. We chose an example corresponding to normal feed conditions of cedar samplings (Fig. 6*b*). The effective extinction coefficient at the excitation wavelength $\sigma(\lambda_l)$ was taken, as in Ref. 33, equal to 0.2 m^{-1}. For such a high optical density, the signal level of spatially resolved LIF rapidly drops. In order to estimate the transformation of the shape of the LIF spectrum, all curves in Fig. 6 are normalized to a single constant. It should be noted that the procedure of modeling of LIF process, proposed earlier,[16] well reproduces the spectral curves of a complex shape. Other details of the Monte Carlo algorithms for imitation of the shortwave radiation transfer in the vegetation cover were discussed in Refs. 33 and 34.

Literature data suggest that presently, the wide-angle means of recording: fibers, fast speed video cameras, and lidars with monochromators are actively used in practical spectrofluorometric studies. In this regard, Figure 7, by the example of LIF spectrum of indol, shows possible consequences of such recording of the spatially resolved LIF spectra.

Figure 7 presents examples of calculation of LIF spectra of indol, excited at $\lambda_l = 0.266$ μm, for different angles of the detector field of view and optical densities of the environment. Spatially resolved LIF spectra are calculated at $\sigma = 0.005$ m^{-1} for the model of foggy haze, containing isotropically distributed fluorescence centers. The optical parameters of the medium for the model of polydisperse liquid droplet aerosol are taken from Ref. 35. The spectrally variable values of $\sigma(\lambda)$ and scattering phase function were calculated in the process of simulation in the spectral region of emission $\Lambda = 350$–525 nm with a step $\Delta\lambda = 5$ nm.

Transformation of the spectra in Fig. 7 reflects relative growth of intensity of the shortwave component of the fluorescent lidar (shift to blue part of spectrum). The transformation of the spectrum is due to increase of contribution of elastic multiple scattering of fluorescent radiation with growth of detector field of view: $\varphi_d = 0.001$; 0.01745; and 0.087 rad. It should be noted that the maximum of curves in Fig. 7*c*, appearing in the shortwave part of

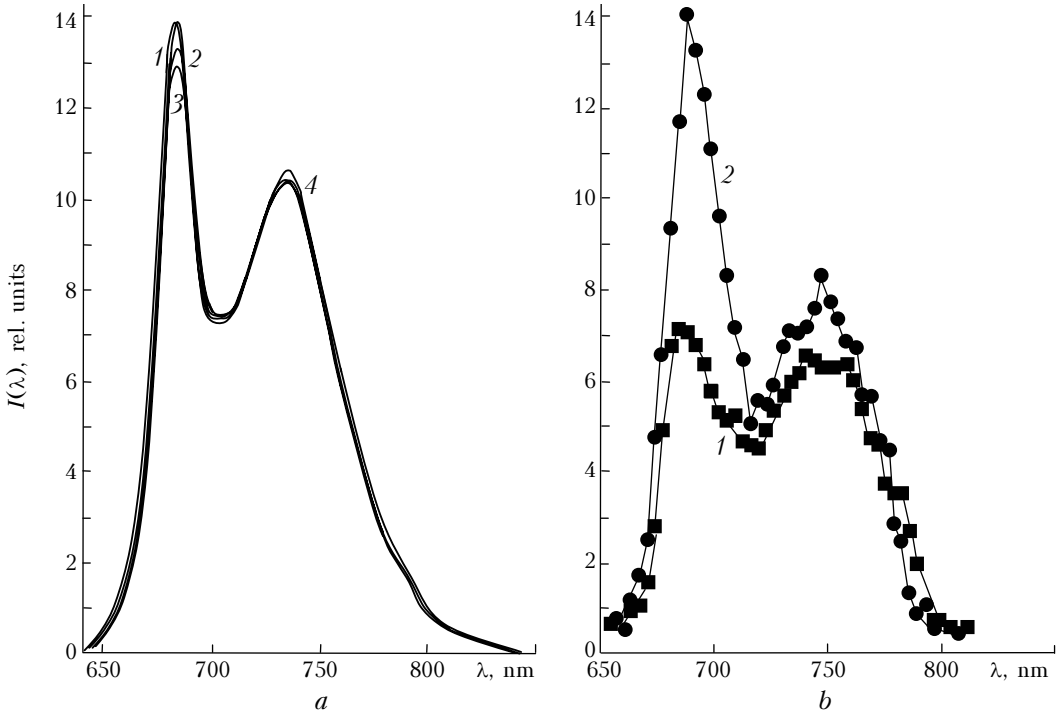

Fig. 6. Calculated LIF spectra of chlorophyll *a* from a homogeneous group of coniferous plants for different depths of signal arrival from distances: 5 (curve *2*), 10 (curve *3*), and 15 m (curve *4*). The effective extinction coefficient $\sigma = 0.2$ m^{-1}; acceptance angle is $\varphi_d = 0.9$ mrad. Curve *1* shows model LIF spectrum, taken from experimental measurements (*a*). Also shown are experimental LIF spectra from a group of cedar saplings: normal feed conditions (curve *1*) and anomalous conditions (curve *2*) (*b*).

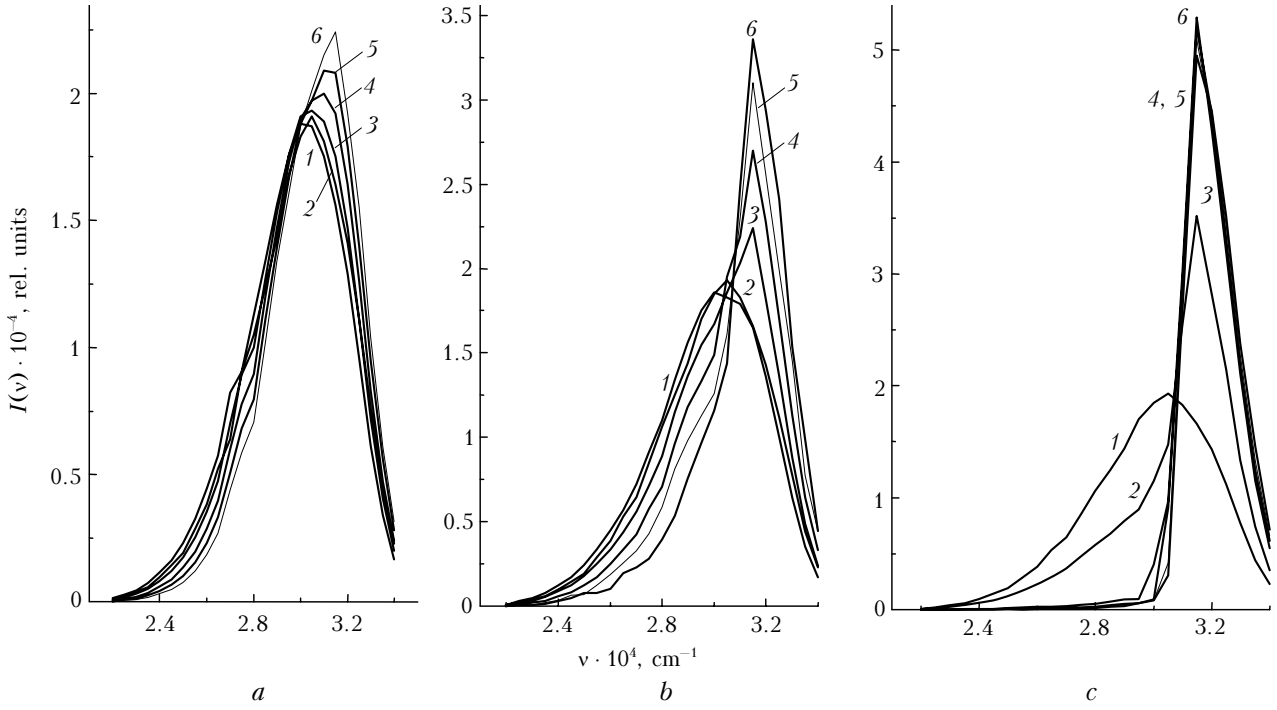

Fig. 7. Spatially resolved LIF spectra of indol for different detector field of view angles and for depths of signal arrival from distances: 50 (curve *1*), 100 (curve *2*), 150 (curve *3*), 200 (curve *4*), 250 (curve *5*), and 300 m (curve *6*). Extinction coefficient $\sigma = 0.005$ m^{-1}; $\varphi_d = 0.001$ (*a*); 0.01745 (*b*); and 0.0874 rad (*c*).

the spectrum, is almost totally caused by multiple scattering signal and carries no useful information on the spectral character of LIF. Therefore, one should exercise caution relative to prospects of using wide-angle systems of the optical detection in lidar systems.

Conclusion

We have briefly analyzed the studies dealing with the use of the phenomenon of laser-induced fluorescence. A constructive description of a modified version of the fluorescent lidar is presented; it is designed for fast remote monitoring of vegetation cover under natural conditions. The lidar offers large functional capabilities owing to use of the second, third, and fourth harmonics of the solid-state YAG laser. We demonstrated the efficiency of fluorescent lidar for remote identification of certain typical forms of the organic aerosol, being the product of the processes of the secondary metabolism of wood plants. It is found that the spectral behavior of LIF well correlates with anomalous deviations of environmental conditions such as in the case of occurrence of aggressive chemical impacts.

In the framework of numerical Monte Carlo simulation, we studied possible distortions of the LIF spectra under conditions of the real turbid atmosphere. The estimates support the necessity of taking into account the multiple scattering background during the use of wide-angle receiving apertures. The limits of quantitative identification of the spectra are established on the basis of the method of artificial neural networks.

Acknowledgements

This work is supported by the Russian Foundation for Basic Research (the grant No. 07–05–00509).

References

1. R. Lacovicz, ed., *Topics in Fluorescence Spectroscopy. Nonlinear and Two-Photons-Induced Fluorescence* (Kluver Acad. Pub., New York, 2002), Vol. 5, 551 pp.
2. A. Harriman, Photochem. **32**, 15–46 (2001).
3. K.Ya. Kondratyev and D.V. Pozdnyakov, *Optical Properties of Natural Waters and Remote Sensing of Phytoplankton* (Nauka, Leningrad, 1988), 183 pp.
4. F.E. Hoge and R.N. Swift, Appl. Opt. **20**, 1191–1201 (1981).
5. M. Bristow, D. Nielson, D. Bundy, and R. Furtek, Appl. Opt. **20**, 2889–2906 (1981).
6. J. Gelbwach and M. Birnbaum, Appl. Opt. **12**, 2442–2447 (1973).
7. C. Weitkamp, ed., *Lidar: Range – Resolved Optical Remote Sensing of the Atmospheric* (Springer Science + Business Media Inc., Singapore, 2005), 451 pp.
8. P. Rairoux, H. Schillinger, S. Niedermeier, M. Rodrigues, and F. Ronneberger, Appl. Phys. **71**, 573–580 (2000).
9. Ch. Buehler, C.Y. Dong, P.T.C. So, T. French, and E. Gratton, Biophys. J. **79**, 536–549 (2000).
10. A. Clericetti, B. Calpini, E. Durieux, and H. Van Bergh, Proc. SPIE **1714**, 291–302 (1992).
11. A.M. Chehalyuk, F.E. Hoge, C.W. Wright, R.N. Swift, and J.K. Yungel, Photosynth. Res. **66**, 35–56 (2000).
12. K.P. Gunter , H.-G. Dahn, and W. Ludeker, Remote Sens. Environ. **47**, 10–17 (1994).
13. A. Ounis, Z.G. Cerovic, J.M. Briantais, and I. Moya, Remote Sens. Environ. **76**, 3–48 (2001).

14. P.H. Kaye, J.E. Barton, E. Hivst, and J.M. Clarc, Appl. Opt. **39**, 3738–3745 (2000).
15. S.C. Hill, R.G. Pinnick, S. Niles, N.F. Fell, Y. Pan, J. Bottiger, B.V. Bronk, and S. Holler, Appl. Opt. **41**, 4432 (2002).
16. A.I. Grishin, G.G. Matvienko, O.V. Kharchenko, V.I. Timofeev, V.M. Klimkin, V.G. Sokovikov, and A.P. Zotikova, Atmos. Oceanic Opt. **12**, No. 4, 320–323 (1999).
17. Y. Saito, M. Kanoh, K. Hatake, T. Kawahara, and A. Nomura, Appl. Opt. **37**, 431–437 (1998).
18. S. Balichenko, A. Dudelzak, and L. Poryvkina, Proc. EARSel **3**, 1–7 (2004).
19. P.C. Gray, I.R. Shokair, S.E. Rosental, G.C. Tisone, Y.S. Wagner, and L.D. Rigdon, Appl. Opt. **37**, 6037–6041 (1998).
20. S. Cristesen, C. Merrow, M. DeSha, and A. Wong, Proc. SPIE **2222**, 228–237 (2004).
21. V.V. Fadeev, T.A. Dolenko, E.V. Filippova, and V.V. Chubarov, Opt. Commun. **166**, 25–33 (1999).
22. U. Shreiberg, Photosynth. Res. **9**, 261–272 (1986).
23. S.A. Dolenko, I.V. Gerdova, T.A. Dolenko, and V.V. Fadeev, Quant. Electron. **31**, 834–838 (2001).
24. D. Moshon, E. Vrindts, B. Ketelaere, J. Baerdemaek, and H. Ramon, Comput. and Electronic in Agricult. **31**, 5–16 (2001).
25. G.M. Krekov and M.M. Krekova, Atmos. Oceanic Opt. **20**, No. 2, 134–140 (2007).
26. A.I. Grishin, G.G. Matvienko, O.V. Kharchenko, and V.I. Timofeev, Atmos. Oceanic Opt. **10**, No. 7, 503–506 (1997).
27. H.K. Lichtenthaler and J.A. Miehe, Trends in Plant Sci. **2**, 316–320 (1997).
28. N.L. Fateyeva, A.V. Klimkin, O.V. Bender, A.P. Zotikova, and M.S. Yamburov, Atmos. Oceanic Opt. **19**, Nos. 2–3, 189–192 (2006).
29. C.M. Bishop, *Neural Networks for Pattern Recognition* (Oxford University Press, 1995), 272 pp.
30. M.Yu. Kataev and A.Ya. Sukhanov, Atmos. Oceanic Opt. **16**, No. 12, 1020–1023 (2003).
31. G.M. Krekov, M.M. Krekova, G.G. Matvienko, A.V. Kovshov, and A.Ya. Sukhanov, Atmos. Oceanic Opt. **20**. No. 3, 237–247 (2007).
32. D.E. Rumelhart, J.L. McClelland, and the PDP Research Group, *Parallel Distributed Processing: Explorations in the Microstructure of Cognition* (Cambridge, MA: MIT Press, 1986), V. 1–2, 550 pp.
33. G.M. Krekov, M.M. Krekova, and G.G. Matvienko, in: *Proc. of XIII Int. Sympos. "Atmospheric Oceanic Optics"* (Tomsk, 2006), 127–128 pp.
34. V.S. Antyufeev, *Monte Carlo Methods for Solving Inverse Problems of Radiation Transfer,* ISSN 90-6764-320-3. 2000. 190 pp.
35. V.E. Zuev and G.M. Krekov, *Optical Models of the Atmosphere* (Gidrometeoizdat, Leningrad, 1986), 256 pp.
36. A.I. Grishin, V.M. Klimkin, G.M. Krekov, M.M. Krekova, G.G. Matvienko, P.A. Palyanov, and N.L. Fateyeva, *"Testbed of laser remote diagnostics of biosystems for study of correlations between optical properties and state of living activity of photosystems,"* Scientific-technical report according to governmental contract No. 02.452.11.7087 of 12.04.2006 (Tomsk, IAO SB RAS, 2006), 231 pp.